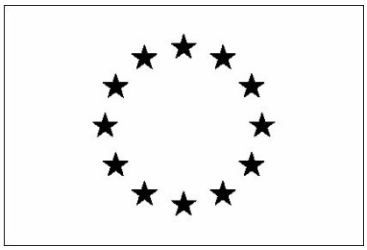

Grant Agreement number: **248095**

Project acronym: **Q-ESSENCE**

Project title: **Quantum Interfaces, Sensors, and Communication based on Entanglement**

Funding Scheme: **Collaborative Project (Large-Scale Integrating Project)**

DELIVERABLE REPORT

Deliverable no.:	**D1.2.3**
Deliverable name:	***Review of quantum sensing beyond the classical limits***
Workpackage no.	**WP1.2**
Lead beneficiary	**UWAW**
Nature	**R = Report**
Dissemination level	**PU = Public**
Delivery date from Annex I (proj month)	**30/04/2013**
Actual / forecast delivery date	**30/04/2013**
Status	**Submitted**

D1.2.3
Review of quantum sensing beyond the classical limits

Review the state of the art achieved in quantum sensing with both photonic and atomic methods

In [KD1-13] applicability and effectiveness of various methods of calculating the ultimate quantum metrological precision bounds resulting from the presence of decoherence are compared. A number of seemingly unrelated concepts have been put into a common framework and an explicit hierarchy of quantum metrological methods in terms of the tightness of the bounds they provide have been presented. In particular, a way to extend the techniques originally proposed in Demkowicz-Dobrzanski et al 2012 Nat. Commun. 3 1063 [DGK1-12], has been shown so that the methods can be efficiently applied not only in the asymptotic but also in the finite-number of particles regime. As a result a simple and direct method has been obtained yielding bounds that interpolate between the quantum enhanced scaling characteristic for small number of particles and the asymptotic regime, where quantum enhancement amounts to a constant factor improvement. Methods have been applied to numerous models including noisy phase and frequency estimation as well as the estimation of the decoherence strength itself.
The methods studied are applicable to models were noise acts independently on the particles and can the problem of quantum sensing can therefore be regarded as a channel estimation problem were channels act in parallel, as show in Figure 1

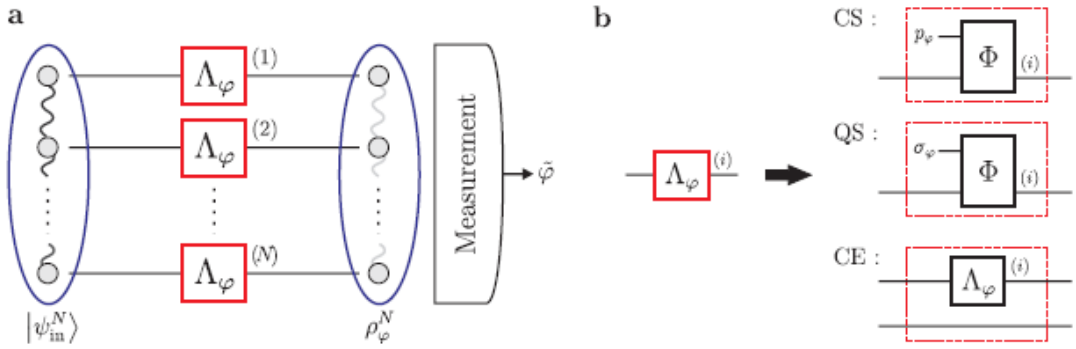

Figure 1 (a) General scheme of quantum metrology with noise acting independently on each of the probes (b) Replacing a channel with either classical simmulation (CS), quantum simmulation (QS) or channel extnesion (CE) allows for a simple derrivation of ultimate bounds on maximal quantum enhancement

Noise model	$\mathcal{F}[\Lambda_\varphi]$	$\mathcal{F}[\Lambda_\varphi \otimes \mathcal{I}]$	$\mathcal{F}_{\text{as}}^{\text{CE}}$ in [39]	$\mathcal{F}_{\text{as}}^{\text{QS}}$	$\mathcal{F}^{\text{RLD}}[\Lambda_\varphi \otimes \mathcal{I}]$	$\mathcal{F}_{\text{as}}^{\text{CS}}$ in [39]
Dephasing	η^2	η^2	$\frac{\eta^2}{1-\eta^2}$	$\frac{\eta^2}{1-\eta^2}$	$\frac{\eta^2}{1-\eta^2}$	$\frac{\eta^2}{1-\eta^2}$
Depolarization	η^2	$\frac{2\eta^2}{1+\eta}$	$\frac{2\eta^2}{(1-\eta)(1+2\eta)}$	$\frac{2\eta^2}{(1-\eta)(1+2\eta)}$	$\frac{2\eta^2(1+\eta)}{(1-\eta)(1+3\eta)}$	$\frac{4\eta^2}{(1-\eta)(1+3\eta)}$
Loss	η	η	$\frac{\eta}{1-\eta}$	$\frac{\eta}{1-\eta}$	n.a.	n.a.
Spontaneous emission	η	$\frac{4\eta}{\left(1+\sqrt{\eta}\right)^2}$	$\frac{4\eta}{1-\eta}$	n.a.	n.a.	n.a.

Table 1 Noise models of metrological relevance are listed in the first column. Decoherence strength increases with a decrease of the η parameter (0 ≤ η < 1. From left to right — single channel QFI; extended channel QFI;

upper bounds on asymptotic channel QFI (per particle used) in ascending order: channel extension bound, quantum simulation bound, RLD-based bound, classical simulation bound

A number of upper bounds on asymptotic (per particle) Quantum Fisher Information (QFI) resulting from the application of various methods have been derived for different decoherence models, see Table 1. The methods have been ordered in a hierarchy with respect to the tightness of the bounds they provide and the scope of models to which they may be applied. It has been proven that the RLD method provides in general tighter bounds than the CS methods, whereas the CS and the QS methods are a special cases of the CE method. As a result, it has been shown that the CE method is the most universal tools for derivation of the bounds among all the methods discussed in the literature. Apart from that the CE method has been generalized to provided even tighter bounds on quantum enhanced precision in the regime of finite number of particles, see Figure 2.

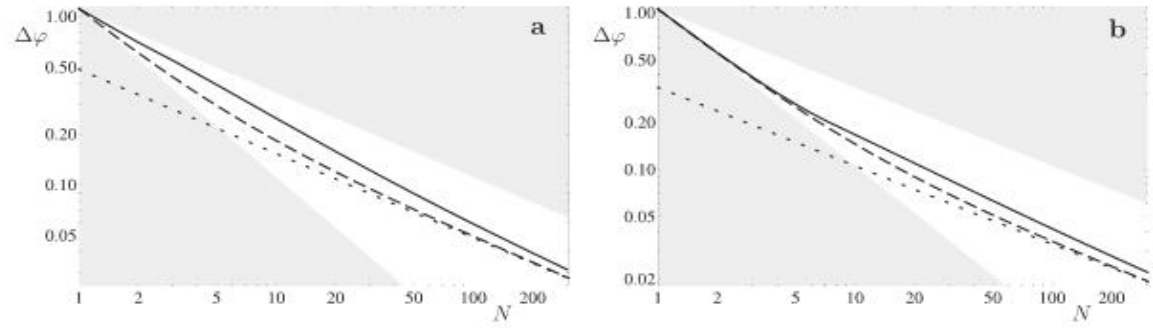

Figure 2 (a) Dephasing: Finite-N (dashed) and the asymptotic CE bounds (dotted) on estimation uncertaintyas compared with the precision achieved by utilizing spin-squeezed states in a Ramsey spectroscopy setup with probe consisting of N atoms experiencing uncorrelated dephasing with η=0.9 (solid). (b) Loss: Lossy interferometry with particle survival probability η=0.9, e.g. Mach-Zehnder interferometer experiencing photonic loss in both of its arms, with effective power transmission η. The smallest uncertainty in a phase estimation scheme is quantified by calculating the QFI for numerically optimized N-particle input states. Again, finite-N (dashed) and asymptotic CE bounds (dotted) on precision are shown for comparison.

Additionally, the problem of frequency rather than phase estimation in the presence of decoherence has been addressed in the framework of continuous quantum evolution described with GKSL (Gorini-Kossakowski-Sudarshan-Lindblad) equations. The issue of the optimal choice of the evolution time has been investigated and expressions for the optimal frequency estimation precision under fixed resources---number of atoms N and the total time of an experiment T---have been derived.

Application of the CS, QS, RLD and CE methods have also been presented to the problem of estimation of the decoherence parameter itself contrasting this problem with the unitary parameter estimation such as phase or frequency. In the case of estimation of the decoherence parameter it has been proven that all the methods considered result in equivalent bounds, hence the simplest and the most intuitive CS method is sufficient for obtaining the optimal bounds for precision.

[**SBM1-12**] Sebastian Steinlechner, Jöran Bauchrowitz, Melanie Meinders, Helge Müller-Ebhardt, Karsten Danzmann, Roman Schnabel, *arXiv:1211.3570.*

[**KD1-13**] J. Kolodynski, R. Demkowicz-Dobrzanski, *Efficient tools for quantum metrology with uncorrelated noise,* arXiv:1303.7271 (submitted to NJP) .

[**CDB1-12**] Philip J. D. Crowley, Animesh Datta, Marco Barbieri, Ian A. Walmsley, *Multiparameter quantum metrology*, arXiv:1206.0043 (Submitted to PRA).

Quantum-Dense Metrology

Sebastian Steinlechner, Jöran Bauchrowitz, Melanie Meinders,
Helge Müller-Ebhardt, Karsten Danzmann, and Roman Schnabel
Institut für Gravitationsphysik, Leibniz Universität Hannover and Max-Planck-Institut für Gravitationsphysik (Albert-Einstein-Institut), Callinstr. 38, 30167 Hannover, Germany
(Dated: November 16, 2012)

Quantum metrology utilizes entanglement for improving the sensitivity of measurements [1, 2]. Up to now the focus has been on the measurement of just *one* out of two non-commuting observables. Here we demonstrate a laser interferometer that provides information about *two* non-commuting observables, with uncertainties below that of the meter's quantum ground state. Our experiment is a proof-of-principle of quantum dense metrology, and uses the additional information to distinguish between the actual phase signal and a parasitic signal due to scattered and frequency shifted photons. Our approach can be readily applied to improve squeezed-light enhanced gravitational-wave detectors at *non*-quantum noise limited detection frequencies in terms of a sub shot-noise veto-channel.

Heisenberg's uncertainty principle states that it is generally not possible to gather precise information about non-commuting observables of a physical system. Prominent examples are the position and the momentum of a particle or the amplitude and phase quadratures of an electro-magnetic wave. In this way the uncertainty of meter systems, e.g. laser light, limits the sensitivity in metrology, even if the quantum mechanical uncertainty of the measurement object itself can be neglected. Using a meter system in a nonclassical state it is, nevertheless, possible to measure one observable with arbitrarily high precision. If its imprecision is 'squeezed' below the zero-point fluctuation of the meter system the regime of quantum metrology is reached, as demonstrated in proof-of-principle experiments [3–10]. Recently, quantum metrology was applied to an operating gravitational wave detector [11].

For a wide application of quantum metrology a rather general problem exists. In order to improve classical state-of-the-art measurement sensitivities, the concept of quantum metrology must be combined with state-of-the-art intense meter states. Current gravitational wave detectors, be they squeezed-light enhanced or not, use light fluxes of about 10^{20} photons per second [12]. Unfortunately, the scattering of just a single photon from the meter into the signal band per second and Hertz produces a significant parasitic signal against which quantum-noise squeezing is bootless. The scatter problem is understood as a *parasitic interference*, where vibrating scatter surfaces frequency-shift a tiny amount of photons into the detection band [13]. It is a well-known problem in high-precision laser interferometry [14–16]. We conjecture that the limitation of quantum metrology at lower detection frequencies as observed in [11] at least partially originates from parasitic interferences. In the future, even higher photon fluxes will be used [17], and parasitic interferences will become increasingly severe.

Here we propose *quantum-dense metrology* (QDM) to widen the application of quantum metrology into the regime where parasitic interferences are a limiting noise source. We present a proof of principle experiment that discriminates between the actual science signal and a parasitic interference with sub-shot-noise measurement precision, exploiting the generally different phase space orientation of the two. It is shown that QDM provides a non-classical veto-channel during signal searches and is thus able to improve a non-classical interferometer beyond what is possible with conventional quantum metrology.

Our readout scheme is based on Einstein-Podolsky-Rosen entanglement [18], which has been first considered for metrology by D'Ariano *et al.* [19]. Following this work we replace the single meter state by a bipartite, two-mode-squeezed entangled state, as depicted in Fig. 1. One mode of the entangled system serves as the new meter state, whereas the other mode is kept as an external reference for the measurement device. Since the difference in position and the sum in momentum commute, $[\hat{x}_A - \hat{x}_B, \hat{p}_A + \hat{p}_B] = 0$, it is in principle possible to exactly measure the distance in phase space between the two modes. Thus we overcome the limitation that is set by the Heisenberg Uncertainty Relation for reading out two orthogonal quadratures of a *single* system by performing all measurements in relation to the reference beam. Such measurements have previously also been considered for super-dense coding with the purpose of doubling the capacity of quantum communication channels [20, 21]. The required continuous-variable entangled states were experimentally pioneered by Ou *et al.* [22], see also [23–25] for more recent experiments. In contrast to all previous proposals, QDM as introduced here uses two-mode squeezing of *non*-orthogonal quadratures. We show that this opens a way to optimize the science signal-to-noise ratio.

The measurement problem of reading out two orthogonal quadratures was pioneered by Arthurs and Kelly [26]. For a light field whose (classical) signal is given by a displacement projected onto the quadratures $X(t) = \langle \hat{x}(t) \rangle$

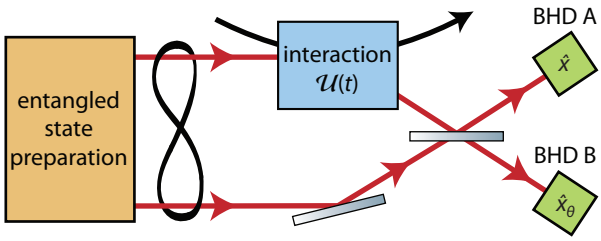

FIG. 1. Schematic showing the underlying principle of quantum-dense metrology. The meter system consists of a bipartite continuous-variable entangled state, of which one part interrogates the system of interest in an interaction zone, while the other part is kept as a local reference. Both entangled modes are recombined after the interaction, and each output is detected via a balanced homodyne detector (BHD).

and $P(t) = \langle \hat{p}(t) \rangle$, the signal-normalized Heisenberg uncertainty relation reads

$$\frac{\Delta^2 \hat{x}(t)}{|X(t)|^2} \frac{\Delta^2 \hat{p}(t)}{|P(t)|^2} \geq \frac{1}{4|X(t)|^2 |P(t)|^2}, \tag{1}$$

where the quadrature variances for the ground state are normalized to $\Delta^2 \hat{x}(t) = \Delta^2 \hat{p}(t) = 1/2$. However, actually measuring both quadratures simultaneously (subscript 'sim') with e.g. an eight-port homodyne detector [27] leads to an uncertainty relation that is four times as large [26],

$$\frac{\Delta^2 \hat{x}_{\rm sim}(t)}{|X_{\rm sim}(t)|^2} \frac{\Delta^2 \hat{p}_{\rm sim}(t)}{|P_{\rm sim}(t)|^2} \geq \frac{1}{|X(t)|^2 |P(t)|^2}. \tag{2}$$

With QDM as presented here, the simultaneous readout is no longer limited by such an uncertainty relation. Instead, the achievable sensitivity is directly connected to the squeezing parameters r_a, r_b of the initial squeezed beams. Entangling those beams with relative angle θ allows for a simultaneous detection of the quadrature $\hat{x}$ and the rotated quadrature $\hat{x}_\theta = \hat{x}\cos\theta + \hat{p}\sin\theta$ with

$$\frac{\Delta^2 \hat{x}^{\rm ent}_{\rm sim}(t)}{|X^{\rm ent}_{\rm sim}(t)|^2} \frac{\Delta^2 \hat{x}^{\rm ent}_{\theta,{\rm sim}}(t)}{|X^{\rm ent}_{\theta,{\rm sim}}(t)|^2} \geq \frac{e^{-2r_a} e^{-2r_b}}{|X(t)|^2 |X_\theta(t)|^2}. \tag{3}$$

Setting $\theta = \pi/2$ the substantial improvement compared to the lower bound in inequality (2) becomes obvious. The Heisenberg uncertainty relation for a conventional readout based on a single-mode meter system (1) is surpassed for two-mode squeezing with $r > 0.3466$. In principle, QDM allows for a readout with arbitrary precision, in the limit of infinite squeezing. A detailed derivation of the above results can be found in the supplementary materials.

We proved the principle of quantum-dense metrology and its high potential for improving state-of-the-art laser interferometers in the following table-top experiment. In a Michelson-type laser interferometer (Fig. 2) with arm lengths of about 7.5 cm we generated two signals in the megahertz regime. The actual interferometer phase signal was produced by modulating the PZT mounted north-arm mirror at 5.55 MHz. We intentionally introduced a parasitic signal at 5.17 MHz by PZT-modulating a small amount of light that leaked through the east-arm mirror. By adjusting the phase with which the light was back-reflected into the interferometer, we were able to simulate a parasitic interferences in any quadrature. The entangled light was generated from two squeezed modes following the scheme in [23]. One mode of the entangled state was introduced into the interferometer dark port via a polarizing beam-splitter (PBS) and a Faraday rotator. The output field was transmitted by the PBS and was overlapped at a 50 : 50 beam-splitter with the other entangled mode. Both beam-splitter outputs were simultaneously detected via balanced homodyne detection (BHD). A more detailed explanation of the experi-

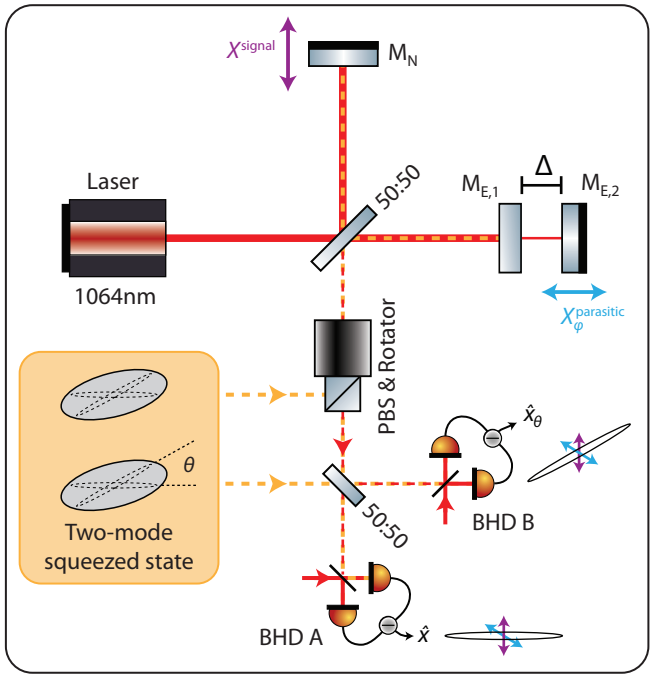

FIG. 2. Schematic setup for the experimental demonstration of quantum dense metrology. Two signals $X^{\rm signal}(t)$ and $X^{\rm parasitic}_\phi(t)$ are generated in a Michelson interferometer by modulating the PZT mounted mirrors M_N and $M_{E,2}$, respectively. $X^{\rm signal}(t)$ is a pure phase modulation, while $X^{\rm parasitic}_\phi(t)$ can be rotated into an arbitrary quadrature by adjusting Δ, which is the microscopic spacing between the east mirrors. A Faraday rotator couples one part of the entangled state into the interferometer. The other part is overlapped with the signal leaving the interferometer. The two resulting beams are simultaneously detected with balanced homodyne detectors, BHD A & B, measuring quadratures $\hat{x}$ and $\hat{x}_{\theta\neq 0}$, respectively $\hat{p} = \hat{x}_{\theta=\pi/2}$. Revealing a parasitic interference requires neither the knowledge of ϕ nor matching θ to ϕ.

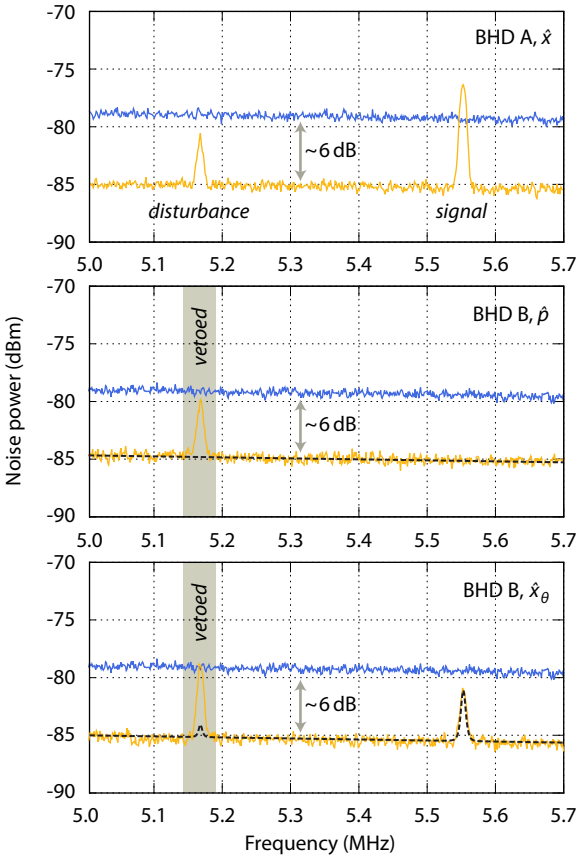

FIG. 3. Experimental demonstration of quantum-dense metrology for the identification of parasitic interferences. The orange traces show the detected signal variances at BHD A, $\Delta^2\hat{x}$ (top panel) and BHD B, $\Delta^2\hat{p}$ (middle) and $\Delta^2\hat{x}_\theta$ (bottom). Parasitic signals are revealed due to their unexpected scaling in the lower two panels. The calculated scalings of science signals are shown in the dashed black curves. In the bottom panel, the angle θ was tuned so that part of the signal was recovered. The blue traces show the vacuum noise power of our BHDs, which are slightly sloped due to the decreasing transfer function of the homodyne detectors. All traces were recorded with RBW 10 kHz, VBW 100 Hz and averaged three times.

mental setup is given in the methods.

The results of our experiment are presented in Fig. 3. The first panel shows the power spectrum of the amplitude quadrature measurement of BHD A, which generally provides the highest signal-to-noise-ratio for the interferometric science signal (here at 5.55 MHz, orange trace). Due to the injected entangled light the readout noise is reduced to 6 dB below the vacuum noise (blue trace). BHD A also clearly detects a second (parasitic) signal at 5.17 MHz. Only by simultaneously looking at $\hat{p}$, as it is done with BHD B (second panel), the parasitic nature of the lower frequency signal is revealed: while the phase signal at 5.55 MHz vanishes as expected, the signal at 5.17 MHz does not vanish but actually increases in size. This information is sufficient to reveal the parasitic nature of the lower frequency signal. Also the second BHD shows readout noise roughly 6 dB below vacuum noise. Simultaneous squeezing in two orthogonal quadratures is unique to our quantum-dense readout scheme.

In the third panel of Fig. 3, we used an improved strategy to reveal the parasitic signal. We detuned the angle θ between the original squeezing ellipses away from 90°. This way it is possible to retain at least part of the science signal in BHD B, while still having insight into the orthogonal quadrature. Since it can be exactly calculated how a phase signal measured at BHD A is projected into the $\hat{x}_\theta$ quadrature, any discrepancy reveals a parasitic signal. The dashed black lines in the second and third panels show the projected noise power, assuming that the first panel contains only phase signals. While the signal at 5.55 MHz perfectly matches the expectation, the disturbance at 5.17 MHz clearly does not. The advantage of the measurement in third panel is that, together with the first panel, the overall signal-to-noise-ratio of the science signal is improved. Changing θ allows for a smooth tuning between full signal coverage ($\theta = 0$), but no information about the conjugate observable; and maximum information about the disturbances in the full phase space ($\theta = \pi/2$), but loss of half the science signal power.

Conclusions — Interference is the basis for many high precision measurements and parasitic interferometer signals are a general problem that hampers the usefulness of nonclassical approaches. We have introduced and experimentally demonstrated the concept of quantum-dense metrology. QDM makes use of the fact that the scientific signal of an interferometer generally appears in a well-determined quadrature. A parasitic interference, however, appears in an arbitrary quadrature orientation. QDM can distinguish between scientific and parasitic signals with unlimited precision beyond the meter's ground state uncertainty, and we proposed and demonstrated that this can be used to create a veto channel for parasitic signals. Our approach uses steady-state entanglement and therefore does not rely on any kind of conditioning or post-selection, which would result in a loss of measurement time. For the first time we propose two-mode squeezing for metrology that is generated with a non-orthogonal relative squeezing angle. Such entangled states allow the optimization of the signal-to-noise ratio when QDM is applied.

Beyond what we have demonstrated here, it should be even possible to subtract parasitic signals from the measurement data without subtracting science signals. For this, two assumptions have to be made. First, the parasitic signals have a quasi-stationary phase space orientation, second, the science signals have a temporal or spectral shape that is different from the parasitic signal. Then, quantum tomography at the second balanced homodyne detector (B) can be used to gather information

about the parasitic signal's phase space orientation and its projected quadrature components. Another idea is keeping the local oscillator phase fixed and introducing a fitting parameter that describes by which magnitude the parasitic signal is projected onto the conventional readout quadrature of the interferometer. Fitting parameters are already used in data analysis based on matched filtering and signal templates [28]. In both scenarios, QDM allows for sub shot-noise measurements even if the apparatus without QDM is limited by parasitic interferences, i.e. is not quantum noise limited. QDM as proposed here does not help in the case of pure parasitic *phase* signals, which are caused by thermally excited fluctuations of mirror surfaces and radiation pressure forces. Instead, it is a valuable tool against all types of parasitic signals having a phase space orientation different from the phase quadrature. Our scheme can be applied to high-precision laser interferometers such as gravitational-wave observatories, where it has high potential in identifying parasitic signals due to photon scattering or hitherto unknown mechanisms. We thus envision that QDM will widen the application of quantum metrology in ongoing and future high precision measurements.

Acknowledgements — We acknowledge discussions with Tobias Eberle, Vitus Händchen and Harald Lück. This research has been financed by the Deutsche Forschungsgemeinschaft (SFB TR7, project C8), the EU FP-7 project Q-ESSENCE and supported by the Centre for Quantum Engineering and Space-Time Research (QUEST) and the IMPRS on Gravitational Wave Astronomy.

[1] V. Giovannetti, S. Lloyd, and L. Maccone, Nature Photonics **5**, 222 (2011).
[2] R. Schnabel, N. Mavalvala, D. E. McClelland, and P. K. Lam, Nature Communications **1**, 121 (2010).
[3] M. Xiao, L.-A. Wu, and H. Kimble, Phys. Rev. Lett. **59**, 278 (1987).
[4] P. Grangier, R. Slusher, B. Yurke, and A. LaPorta, Phys. Rev. Lett. **59**, 2153 (1987).
[5] D. Leibfried, M. D. Barrett, T. Schaetz, J. Britton, J. Chiaverini, W. M. Itano, J. D. Jost, C. Langer, and D. J. Wineland, Science **304**, 1476 (2004).
[6] P. Cappellaro, J. Emerson, N. Boulant, C. Ramanathan, S. Lloyd, and D. Cory, Phys. Rev. Lett. **94** (2005), 10.1103/PhysRevLett.94.020502.
[7] H. Vahlbruch, S. Chelkowski, B. Hage, A. Franzen, K. Danzmann, and R. Schnabel, Physical Review Letters **95**, 1 (2005).
[8] I. Afek, O. Ambar, and Y. Silberberg, Science **328**, 879 (2010).
[9] W. Wasilewski, K. Jensen, H. Krauter, J. J. Renema, M. V. Balabas, and E. S. Polzik, Phys. Rev. Lett. **104**, 1 (2010).
[10] B. Lücke, M. Scherer, J. Kruse, L. Pezzé, F. Deuretzbacher, P. Hyllus, O. Topic, J. Peise, W. Ertmer, J. Arlt, L. Santos, A. Smerzi, and C. Klempt, Science **334**, 773 (2011).
[11] J. Abadie, B. P. Abbott, R. Abbott, T. D. Abbott, M. Abernathy, and et al., Nature Physics **7**, 962 (2011).
[12] A. Abramovici, W. E. Althouse, R. W. Drever, Y. Gürsel, S. Kawamura, F. J. Raab, D. Shoemaker, L. Sievers, R. E. Spero, K. S. Thorne, R. E. Vogt, R. Weiss, S. E. Whitcomb, and M. E. Zucker, Science **256**, 325 (1992).
[13] H. Vahlbruch, S. Chelkowski, K. Danzmann, and R. Schnabel, New Journal of Physics **9**, 371 (2007).
[14] J.-Y. Vinet, V. Brisson, and S. Braccini, Physical Review D **54**, 1276 (1996).
[15] J.-Y. Vinet, V. Brisson, S. Braccini, I. Ferrante, L. Pinard, F. Bondu, and E. Tournié, Physical Review D **56**, 6085 (1997).
[16] D. J. Ottaway, P. Fritschel, and S. J. Waldman, Optics Express **20**, 8329 (2012).
[17] S. Hild, S. Chelkowski, A. Freise, J. Franc, N. Morgado, R. Flaminio, and R. DeSalvo, Classical and Quantum Gravity **27**, 015003 (2010).
[18] A. Einstein, B. Podolsky, and N. Rosen, Physical Review **47**, 777 (1935).
[19] G. M. D'Ariano, P. Lo Presti, and M. G. A. Paris, Phys. Rev. Lett. **87**, 1 (2001).
[20] C. H. Bennett and S. J. Wiesner, Phys. Rev. Lett. **69**, 2881 (1992).
[21] S. L. Braunstein and H. J. Kimble, Phys. Rev. A **61**, 042302 (2000).
[22] Z. Y. Ou, S. F. Pereira, H. J. Kimble, and K. C. Peng, Phys. Rev. Lett. **68**, 3663 (1992).
[23] A. Furusawa, J. L. Sø rensen, S. L. Braunstein, C. A. Fuchs, H. J. Kimble, and E. S. Polzik, Science **282**, 706 (1998).
[24] C. Silberhorn, P. Lam, O. Weiss, F. König, N. Korolkova, and G. Leuchs, Physical Review Letters **86**, 4267 (2001).
[25] W. P. Bowen, R. Schnabel, and P. K. Lam, Phys. Rev. Lett. **90**, 4 (2003).
[26] E. Arthurs and J. L. Kelly, Bell Syst. Tech. J. **44**, 725 (1965).
[27] U. Leonhardt, *Measuring the quantum state of light* (Cambridge University Press, Cambridge, 1997).
[28] B. Sathyaprakash and B. Schutz, Living Rev. Relativity **12** (2009).
[29] S. Steinlechner, J. Bauchrowitz, T. Eberle, and R. Schnabel, "Strong EPR-steering with unconditional entangled states," (2011), arXiv:arXiv:1112.0461.
[30] L. Schnupp, "Presentation at European Collaboration Meeting on Interferometric Detection of Gravitational Waves (Sorrent, Italy)," (1988).

SUPPLEMENTARY MATERIAL

Entangled-light generation. Our continuous-variable entangled light was generated by the source described in [29]. Two squeezed vacuum fields generated by type I parametric down-conversion in PPKTP were overlapped at a 50 : 50 beam splitter, thereby creating two-mode squeezed light. Both input fields carried a residual phase modulation from locking the optical parametric amplifiers. At the detection stage, this modulation was reused to align the homodyne detectors to the

squeezed quadratures. A single sideband modulation was imprinted on one of the squeezed fields by overlapping it with 80 MHz frequency-shifted light from an acousto-optical modulator. This sideband was used to lock the quadrature angle between the input squeezed states. It was also used to stabilize one mode of the entangled field to the Michelson interferometer by detecting the beat signal between the sideband and the interferometer input field behind one end-mirror.

Interferometer setup and control. The Michelson interferometer had an arm length of about 7.5 cm for the north arm. The east arm was about 1.5 cm shorter, which allowed us to use the so-called Schnupp modulation technique [30] for locking the interferometer to its dark fringe. Both end-mirrors were flat and had a power reflectivity of 99.98% (M_N) and 98% (M_{E1}). The north mirror was PZT mounted to create a phase modulation inside the interferometer. A second PZT mounted flat mirror M_{E2} with reflectivity of $\approx 20\%$ was placed a few millimeters behind M_{E1}, creating a (weakly coupled) Fabry-Pérot cavity. By tuning this cavity, the phase signal created by M_{E2} could be rotated into an arbitrary quadrature. A DC locking scheme detected the transmitted light and held the cavity on its operating point. Both PZTs were driven on a mechanical resonance to be able to create signals in the few megahertz regime where the detected squeezing was strongest.

Readout of orthogonal quadratures. Consider a continuous-wave laser beam with central frequency ω_0. The quantum noise of this beam at the sideband frequencies $\pm\Omega$, measured with a resolution bandwidth of $\Delta\Omega$, can be described by time-dependent operators for the amplitude quadrature $\hat{a}_1(\Omega, \Delta\Omega, t)$ and the phase quadrature $\hat{a}_2(\Omega, \Delta\Omega, t)$. Here we restrict ourselves to a monochromatic signal at a fixed sideband frequency and therefore drop the explicit frequency dependency in the following treatment. The quadrature operators satisfy the commutation relation $[\hat{a}_1, \hat{a}_2] = i$ and are normalized such that for a (squeezed) minimum uncertainty state $\Delta^2\hat{a}_1 = \Delta^2\hat{a}_2 = e^{\mp 2r}/2$, where the minus sign in the exponent belongs to the amplitude quadrature and the plus sign to the phase quadrature. r is the squeezing parameter, therefore $r = 0$ corresponds to a vacuum state, while $r < 0$ and $r > 0$ correspond to phase and amplitude squeezed light, respectively.

A measurement adds (classical) amplitude and phase modulations $X(t)$, $P(t)$ to the laser beam. The output field can then be described by the field quadrature vector

$$\hat{\boldsymbol{m}} = \begin{pmatrix} \hat{x}(t) \\ \hat{p}(t) \end{pmatrix} = \begin{pmatrix} \hat{a}_1(t) + X(t) \\ \hat{a}_2(t) + P(t) \end{pmatrix} . \tag{4}$$

From the commutation relation we can infer the Heisenberg uncertainty relation for the shot noise, normalized to the signal,

$$\frac{\Delta^2\hat{x}(t)}{\left|X(t)\right|^2} \frac{\Delta^2\hat{p}(t)}{\left|P(t)\right|^2} \geq \frac{1}{4\left|X(t)\right|^2\left|P(t)\right|^2} . \tag{5}$$

This inequality limits the simultaneous measurability of the amplitude and phase quadrature modulations. A simple approach to actually measure both quadratures in an Arthurs-Kelly type experiment is to split the beam at a 50 : 50 beam splitter – which introduces the vacuum mode $\hat{\boldsymbol{v}}$ – and then simultaneously perform a homodyne detection at each output port. Measuring the amplitude quadrature $\hat{x}_{\rm sim} = (\hat{x} + \hat{v}_1)/\sqrt{2}$ in one detector and the phase quadrature $\hat{p}_{\rm sim} = (\hat{p} - \hat{v}_p)/\sqrt{2}$ in the other leads to

$$\frac{\Delta^2\hat{x}_{\rm sim}(t)}{\left|X_{\rm sim}(t)\right|^2} \frac{\Delta^2\hat{p}_{\rm sim}(t)}{\left|P_{\rm sim}(t)\right|^2} \geq \frac{1 + \cosh(2r)}{2\left|X(t)\right|^2\left|P(t)\right|^2} , \tag{6}$$

where $X_{\rm sim}(t) = X(t)/\sqrt{2}$ and $P_{\rm sim}(t) = P(t)/\sqrt{2}$, since also the signal is divided at the beam splitter. Equation (4) states that the achievable minimum uncertainty is indeed at least four times larger than the limit imposed by Eq. (3). Squeezing does not help in this measurement scenario and the best sensitivity is achieved with vacuum input, i.e. $r = 0$.

For QDM, consider two squeezed vacuum modes with squeezing parameters r_a and r_b, described by the quadrature vectors $\hat{\boldsymbol{a}}$ and $\hat{\boldsymbol{b}}$. For simplicity, we restrict ourselves to the case where beam $\hat{\boldsymbol{a}}$ is always squeezed in the amplitude quadrature and the other beam is rotated in the quadrature space by θ. After entangling these beams at a 50 : 50 beam splitter, one mode is used as the meter state $\hat{\boldsymbol{m}}$ which is modulated with the signals $X(t)$, $P(t)$ as above, while the other state $\hat{\boldsymbol{r}}$ is kept as a reference beam. These two modes are then recombined at another beam splitter, whose two output fields are sent to balanced homodyne detectors A and B measuring the quadrature fields

$$\hat{x}^{\rm ent}_{\rm sim} = \frac{1}{\sqrt{2}}(\hat{r}_1 - \hat{x}) = \hat{a}_1 - X^{\rm ent}_{\rm sim}(t) , \tag{7}$$

and

$$\hat{x}^{\rm ent}_{\theta,\rm sim} = \frac{1}{\sqrt{2}}(\hat{r}_\theta + \hat{x}_\theta) = \hat{b}_\theta + X^{\rm ent}_{\theta,\rm sim}(t) , \tag{8}$$

respectively. Here, $\hat{x}_\theta = \hat{x}\cos\theta + \hat{p}\sin\theta$, $X_\theta(t) = X(t)\cos\theta + P(t)\sin\theta$ and the signals are again scaled by $1/\sqrt{2}$ since they are equally divided between the two homodyne detectors. The corresponding uncertainty product reads

$$\frac{\Delta^2\hat{x}^{\rm ent}_{\rm sim}(t)}{\left|X(t)\right|^2/2} \frac{\Delta^2\hat{x}^{\rm ent}_{\theta,\rm sim}(t)}{\left|X_\theta(t)\right|^2/2} = \frac{e^{-2r_a}e^{-2r_b}}{\left|X(t)\right|^2\left|X_\theta(t)\right|^2} . \tag{9}$$

This uncertainty is not bounded from below, for $r_a, r_b \to \infty$. Thus we have shown that quantum-dense metrology, which is performed in relation to a reference beam, can in principle reach arbitrarily high signal-to-noise ratios.

Multiparameter quantum metrology

Philip J. D. Crowley, Animesh Datta,* Marco Barbieri, and Ian A. Walmsley
Clarendon Laboratory, Department of Physics, University of Oxford, OX1 3PU, United Kingdom
(Dated: June 25, 2012)

Interferometry is an experimental paradigm underlying a range of applications from atomic clocks to gravitational wave detection and cell-membrane dynamics. The fundamental limit on estimating path differences in interferometers is set by the resources available - the volume of space-time, energy, number of particles - through the Cramér-Rao bound. Different metrological schemes are judged by the scaling of the estimator's uncertainty in the resources consumed. Quantum probes are known to provide enhanced precision in single-parameter estimation. However, multiparameter quantum interferometry remains largely unexplored. Here we show that estimating one parameter with quantum-limited precision inexorably leads to a reduced precision of the other. Unlike single-parameter estimation, it is impossible to design a strategy saturating the quantum Cramér-Rao bound for loss and phase estimation in a single setup simultaneously. We design optimal quantum states achieving the best possible simultaneous precisions. Our results reveal general features about concurrently estimating hamiltonian and dissipative parameters, and can be applied to sophisticated sensing scenarios such as quantum imaging.

A vast majority of metrological problems, particularly those associated with hamiltonian dynamics, can be recast into one of phase estimation [1, 2]. In the optical domain, high accuracy measurements of the path differences, characterized by a phase difference ϕ between the two modes of the apparatus, have found use in many fields [3–6], and has consistently featured as an important tool in physics, from the null result in the search for luminiferous aether [7] to detecting small variations in the refractive index of biological solutions [8–11]. Most of these experiments estimate a single parameter, the phase difference [12–16]. Quantum states of a few photons promise enhanced precision in single parameter estimation compared to the best classical strategies [17, 18]. In this case, the quantum limit for estimation is always attainable [13]. This enhanced quantum precision is reflected in the improved scaling of the variance of the estimator with the number of particles, which is the primary resource in most quantum metrological schemes.

Phase shifts are generated by Hamiltonian evolution of the particles. The most general evolution however, comprises both Hamiltonian and dissipative dynamics. In an interferometric setup, this requires the estimation of phase and loss parameters that characterise these two elements of the evolution. The problem of estimating multiple parameters for such evolution is still nascent [19–24]. It clearly has important technological implications, not only because all practical systems exhibit loss, but also because there are many situations in which multiple parameters of several kinds are the objective of the experimenter. This is the case, for instance, where both dispersion and absorption profiles of a sample are sought with high accuracy using a single experimental set up. While one can estimate the parameters independently, this demands the preparation of different optimal probe states and measurements for each parameter. This is tantamount to arranging a different experimental setup for each parameter and requires a full reconfiguration, which may be technically demanding. Furthermore sequential estimation is not effective for sensing time-varying samples. These limitations are overcome by simultaneous estimation of both parameters.

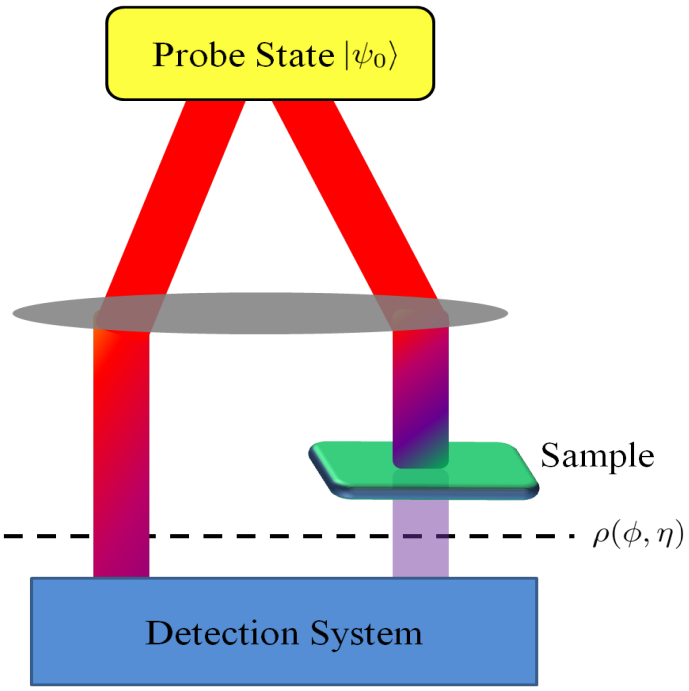

FIG. 1. Schematic of an imaging system : A two-mode n-photon quantum probe state $|\psi_0\rangle$ irradiates the sample and provides the reference arm of a two-port interferometer. The detection is chosen so to estimate simultaneously the phase shift ϕ (Hamiltonian dynamics) and the transmission η (dissipative dynamics) from the state $\rho(\phi,\eta)$ resulting from the interaction of the probe with the sample.

In this Letter, we analyse this measurement strategy, and derive fundamental limits for the precision with which phase and loss in an interferometer can be estimated in a single apparatus. We show that it is not possible to attain the individual quantum limits of the two parameters at the same time. The optimal strategy involves a trade-off between the individual quantum precision bounds, revealing how quantum mechanics forbids their simultaneous saturation. The practical task of

accomplishing the optimal precision requires the identification of appropriate quantum probes. To that end, we provide the design of optimal two-mode quantum states with a fixed number of photons that gets closest to the ultimate quantum limit of simultaneous phase and loss estimation, by explicit numerical optimization for low photon numbers. For samples with high losses, it is natural to use states with a high particle flux, and in this limit we present an analytic expression for the profile of the optimal quantum probes.

The archetypal schema for quantum sensing is illustrated in Fig. (1). An object, characterized by a set of parameters $\boldsymbol{\theta} = \{\theta_\nu\}$, is placed in one of the arms of a Mach-Zehnder interferometer. This extends the simple case in which a single phase shift contains the only relevant information, to a more realistic case, in which, for example, both the phase shift and the loss are important. The initial probe evolves upon propagation through the system, acquiring a form that depends on the parameter set. At the output, measurements of the probe state provide a multivariate probability distribution that captures changes in the state due to changes in the system parameter. The optimal probe state is one for which the derivative of the probability distribution with respect to these parameters is largest.

For a single parameter, it is possible to identify the optimal measurement by analysing the quantum Fisher information. This is constructed using the symmetric logarithmic derivative (SLD), which quantifies the changes of the state with respect to the system parameters, and also provides a means to identify the optimal probe states and measurement strategies that saturate the quantum limit to precision, which is given by the quantum Cramér-Rao bound. [13]. In the multiparameter case, the variation with each parameter can be measured by SLDs corresponding to each of the different parameters. The information concerning the parameters $\boldsymbol{\theta}$ that can be obtained from the set of any and all possible measurements is then encapsulated in the quantum Fisher information matrix [25]. The covariance matrix, the multivariate version of the variance of the estimator, is bounded by the inverse of the quantum Fisher information matrix through the quantum Cramér-Rao bound [25].

The quantum Fisher information matrix involving a pair of parameters generating Hamiltonian and dissipative dynamics is necessarily diagonal, because the tangent spaces corresponding these two types of dynamics are orthogonal. The corresponding covariance matrix for such a pair of parameters is diagonal when the quantum Cramér-Rao bound is saturated. The matrix inequality that defines the quantum Cramér-Rao bound does not, however, take into account the non-commutativity of quantum operators, which may prevent it from being saturated (See Supplementary Information). A diagonal covariance matrix implies the statistical independence of the parameters. This general feature suggests that Hamiltonian and dissipative parameters may be estimated simultaneously at quantum limit, with their respective uncertainties given by the inverse of the diagonal elements, as is the case for the quantum Fisher information matrix for phase and loss estimation. Yet, it is not so, as we show in the next section. This makes multiparameter quantum metrology nontrivial, and fundamentally different not only from classical multiparameter estimation, but also quantum single parameter estimation, as in both these cases the Cramér-Rao bound can always be saturated.

The best probes states are the ones that maximize the quantum Fisher information. Since particle number being a central resource in quantum metrology, we specify the probe states as the most general normalised pure states of a fixed particle number, which are of the form

$$|\psi_0\rangle = \sum_{k=0}^{n} \sqrt{x_k}|k, n-k\rangle. \tag{1}$$

The covariance matrix for the phase shift ϕ (ranging between 0 and 2π) and loss η (ranging between 0 for complete absorption and 1 for complete transmission of the probe light) associated with the Hamiltonian and dissipative components of the states evolution is diagonal when the quantum Cramér-Rao bound is saturated. In particular, the quantum Fisher information matrix is given by

$$\mathcal{I}[\rho] = \begin{pmatrix} \mathcal{I}_{\phi\phi} & 0 \\ 0 & \mathcal{I}_{\eta\eta} \end{pmatrix}, \tag{2}$$

where $\mathcal{I}_{\phi\phi}, \mathcal{I}_{\eta\eta}$ are the quantum Fisher information for the estimation of phase and loss respectively. Defining $\xi_{r,s} = \sum_{t=s}^{n} x_t b_s^t t^r$, $\Xi_r = \sum_{t=0}^{n} x_t t^r$, being the moments of the coefficients of x_t, and b_s^t is a binomial factor [26],

$$\mathcal{I}_{\phi\phi} = 4\left(\Xi_2 - \sum_{l=0}^{n} \frac{\xi_{1,l}^2}{\xi_{0,l}}\right), \quad \mathcal{I}_{\eta\eta} = \frac{\Xi_1}{\eta(1-\eta)}, \tag{3}$$

It is easy to conclude the form of the optimal states for the estimation of loss and phase independently. In the absence of losses, $\eta = 1$, $b_s^t = \delta_{s,0}$, $\mathcal{I}_{\phi\phi}^{(\eta=1)} = 4\left(\Xi_2 - \Xi_1^2\right)$, which is the variance of x_k, maximised for a $n00n$ state, when $\mathcal{I}_{\phi\phi}^{(\eta=1)} \sim n^2$, as is well-known. In the lossy case, the best states for estimation of phase are arrived at by maximizing the general form of $\mathcal{I}_{\phi\phi}$ [15, 27, 28]. On the other hand, the best state for estimating the loss is the Fock state $|n, 0\rangle$, in which case $\mathcal{I}_{\eta\eta} \sim n$ [29, 30]. For η=0, 1 the quantum Fisher information for loss $\mathcal{I}_{\eta\eta}$ diverges. This is also to be expected as in these cases all the photons are lost or all transmitted, so that the variance in the outcomes of measurements of particle number in these cases will be zero.

The necessary condition for saturating the multiparameter quantum Cramér-Rao bound, derived using techniques of local asymptotic normality, is given by the expectation value of the commutator of the two SLDs [31]. In our case, this reduces to

$$\mathrm{Tr}\left[\rho[L_\eta, L_\phi]\right] = -i\frac{\mathcal{I}_{\phi\phi}}{2\eta}. \tag{4}$$

This implies that the optimal measurements necessary to attain the quantum limits for the two parameters do not commute, and it is impossible to estimate the phase and loss using

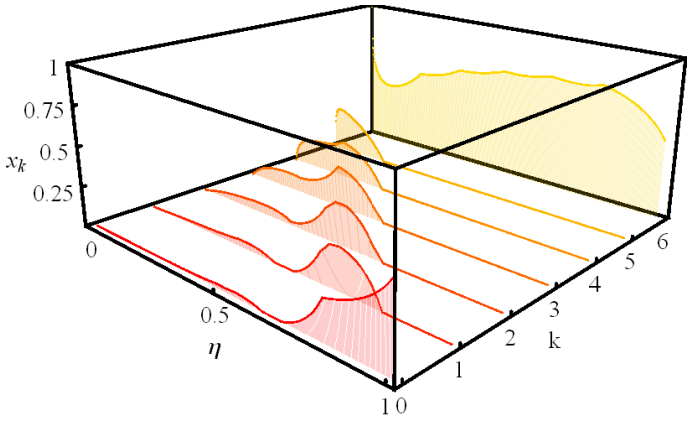

FIG. 2. Coefficients of the optimal probe states of the form in Eq. (1) for $n = 6$ obtained by numerical optimisation. The state resembles the optimal probes for phase estimation in the presence of losses [15], and interpolates towards the Fock state $|6, 0\rangle$, optimal state for estimating η.

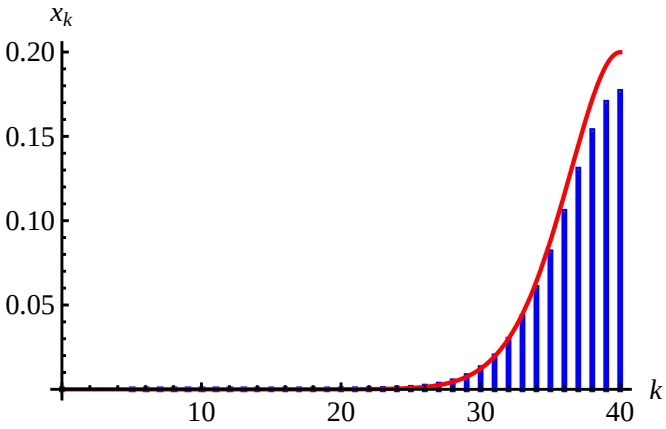

FIG. 3. Comparison of the coefficients of the optimal states from the analytical and numerical procedures, for $n = 40, \eta = 0.02, w = 0.9$. The red solid line corresponds to Eq. (6).

quantum probes with a fixed photon number. The only instance when the quantum Cramér-Rao bound *can* be saturated is when we learn nothing of the phase ϕ. One could still estimate the loss parameter η in this situation, using as probe the Fock state $|n, 0\rangle$. Evidently, this state and the corresponding SLD has no sensitivity to the phase in the interferometer. More generally, no phase information can be extracted using a fixed photon number state as in Eq. (1) and measurements derived from the loss SLD [26].

The only option now left is to use the SLD for phase estimation to estimate the loss parameter. This at least guarantees the quantum limit for one of the parameters, while any other measurement will be suboptimal for both. Having thus chosen the SLD for phase to estimate the loss, the classical Fisher information is [26]

$$I_{\eta\eta} = \mathcal{I}_{\eta\eta} - \frac{1}{4\eta^2}\mathcal{I}_{\phi\phi}. \tag{5}$$

This result brings to light another interesting trade-off. It shows that the precision of loss estimation can only be enhanced at the cost diminished precision in estimating the phase, and vice-versa. In spite of this tradeoff, there is an asymmetry between the two parameters. Estimating loss at the quantum limit requires a complete sacrifice in estimating phase, but phase estimation at the quantum limit leaves us with some information about loss. Thus, quantum mechanics limits the estimation of Hamiltonian and dissipative parameters at the quantum limit differently, given by Eqns. (3) and (5).

In addition to the conceptual understanding of quantum trade-offs and limitations that this analysis provides, the practical challenge in any multiparameter estimation scenario such as imaging in Fig. (1) lies in identifying the quantum probes that maximize the precisions of both the parameters simultaneously to the best possible extent. For a single parameter, maximizing the quantum Fisher information is tantamount to minimizing the uncertainty. For multiparameter quantum metrology, the sum of the variances of all the parameters is bounded from below by the trace of the inverse of the quantum Fisher information matrix. In our case of a diagonal Fisher information matrix, the optimal probes are then given by the minimization of the sum of the reciprocals of $\mathcal{I}_{\phi\phi}$ and $I_{\eta\eta}$ given by Eqns. (3) and (5). For low particle numbers, this minimization can be performed numerically, and the result for $n = 6$ is presented in Fig. (2). An alternative criterion of choosing the optimal probe states is to maximize the Fisher information corresponding to the two parameters. More generally, their convex combination which assigns different weights to the different parameters can be maximized, and we do so in a novel context next.

Going beyond the current state-of-the-art of few-particle quantum probes in quantum metrology [11, 18], we look to the future of quantum imaging and sensing involving high-loss samples and scenarios such as highly scattering media [32] or long-distance quantum interferometers [33]. In these cases, high flux probe states are necessary and an explicit numerical optimization inadequate. An asymptotic analytic form of the coefficients in this case is given by [26]

$$x_k \approx \frac{1}{n\gamma|\zeta_0|\mathrm{Ai}^2(\zeta_0)}\mathrm{Ai}^2\left(\frac{1}{\gamma} - \frac{k}{\gamma n} + \zeta_0\right), \tag{6}$$

where $\gamma^3 = \frac{4\eta(2w-1)}{n(1-\eta)^2 w}$, and ζ_0 is the smallest zero of the first derivative of the Airy function $\mathrm{Ai}(y)$. w is the weight assigned to the phase parameter, and in this limit, the precisions of estimating the phase and loss when using the optimal state scales as [26]

$$\mathcal{I}_{\phi\phi} = \frac{4\eta}{1-\eta}n - \mathcal{O}(n^{2/3}), \quad I_{\eta\eta} = \frac{|\zeta_0|}{3}\beta n^{2/3}. \tag{7}$$

where $\beta = (2w/\eta(1-\eta)(2w-1))^{2/3}$. The linear scaling of the quantum Fisher information with the number of photons in the probe state for the estimation of phase is the best

possible in the high loss regime [34]. In Fig. (3), we plot the asymptotic profile of the probe states for a high flux, high loss scenario, and compare it with explicit numerical computation of the coefficients. The similarities between the two profiles shows the qualitative and quantitative equivalence between estimating different sets of parameters using the measurements derived from the phase SLD .

We have shown how quantum mechanics limits the simultaneous estimation of multiple parameters at the quantum limit. In particular, we have illustrated that the estimation of a pair of parameters describing the Hamiltonian and the dissipative evolution of a probe state in an interferometric sensor cannot give both parameters at the simultaneous quantum limit of each. This situation is relevant to a broad range of sensors, and opens the door to more complex quantum imaging devices, in which multiple parameters related to the object configuration are sought. Although the saturation of the multiparameter quantum Cramér-Rao predicts a diagonal covariance matrix, suggesting statistically independent parameters, we show that they cannot be estimated concurrently at the quantum limit. Furthermore, the best possible strategy imposes a trade-off between the attainable precisions of the two parameters. This trade-off forces an optimization strategy to determine the form of best quantum probes for multiparameter quantum metrology at the ultimate attainable limit.

ACKNOWLEDGEMENTS

We thank M. Guta, J. Nunn, X. Jin, L. Zhang for stimulating and informative discussions. This work was funded in part by EPSRC (Grant No. EP/H03031X/1), U.S. EOARD (Grant No. 093020), EU Integrated Project QESSENCE. MB is supported by a FASTQUAST ITN Marie Curie fellowship. IAW acknowledges support from the Royal Society.

* animesh.datta@physics.ox.ac.uk

[1] V. Giovannetti, S. Lloyd, and L. Maccone, Science, **306**, 1330 (2004).
[2] V. Giovannetti, S. Lloyd, and L. Maccone, Nature Photonics, **5**, 10 (2011).
[3] W. Steel, *Interferometry*, Cambridge Studies in Modern Optics (Cambridge University Press, 1983).
[4] J. Ye, H. Schnatz, and L. Hollberg, Selected Topics in Quantum Electronics, IEEE Journal of, **9**, 1041 (2003).
[5] B. Abbott *et al.* (LIGO Scientific Collaboration), Phys. Rev. Lett., **95**, 221101 (2005).
[6] C. Yang, A. Wax, M. S. Hahn, K. Badizadegan, R. R. Dasari, and M. S. Feld, Opt. Lett., **26**, 1271 (2001).
[7] A. A. Michelson and E. W. Morley, American Journal of Science, **34**, 333 (1887).
[8] B. J. Luff, J. S. Wilkinson, J. Piehler, U. Hollenbach, J. Ingenhoff, and N. Fabricius, J. Lightwave Technol., **16**, 583 (1998).
[9] S. Watts, Nature Photonics, **4**, 433 (2010).
[10] A. Pierangelo, A. Benali, M.-R. Antonelli, T. Novikova, P. Validire, B. Gayet, and A. D. Martino, Opt. Express, **19**, 1582 (2011).
[11] A. Crespi, M. Lobino, J. C. F. Matthews, A. Politi, C. R. Neal, R. Ramponi, R. Osellame, and J. L. O'Brien, arxiv:1109.3128 (2011).
[12] M. J. Holland and K. Burnett, Phys. Rev. Lett., **71**, 1355 (1993).
[13] S. L. Braunstein and C. M. Caves, Phys. Rev. Lett., **72**, 3439 (1994).
[14] J. J. . Bollinger, W. M. Itano, D. J. Wineland, and D. J. Heinzen, Phys. Rev. A, **54**, R4649 (1996).
[15] U. Dorner, R. Demkowicz-Dobrzanski, B. J. Smith, J. S. Lundeen, W. Wasilewski, K. Banaszek, and I. A. Walmsley, Phys. Rev. Lett., **102**, 040403 (2009).
[16] A. Datta, L. Zhang, N. Thomas-Peter, U. Dorner, B. J. Smith, and I. A. Walmsley, Phys. Rev. A, **83**, 063836 (2011).
[17] M. W. Mitchell, J. S. Lundeen, and A. M. Steinberg, Nature, **429**, 161 (2003).
[18] N. Thomas-Peter, B. J. Smith, A. Datta, L. Zhang, U. Dorner, and I. A. Walmsley, Phys. Rev. Lett., **107**, 113603 (2011).
[19] E. Bagan, M. Baig, and R. Muñoz Tapia, Phys. Rev. A, **70**, 030301 (2004).
[20] G. Chiribella, G. M. D'Ariano, P. Perinotti, and M. F. Sacchi, Phys. Rev. Lett., **93**, 180503 (2004).
[21] H. Imai and A. Fujiwara, Journal of Physics A: Mathematical and Theoretical, **40**, 4391 (2007).
[22] A. Monras and F. Illuminati, Phys. Rev. A, **83**, 012315 (2011).
[23] A. Chiuri, V. Rosati, G. Vallone, S. Pádua, H. Imai, S. Giacomini, C. Macchiavello, and P. Mataloni, Phys. Rev. Lett., **107**, 253602 (2011).
[24] R. Blandino, M. G. Genoni, J. Etesse, M. Barbieri, M. G. A. Paris, P. Grangier, and R. Tualle-Brouri, arxiv:1203.1127 (2012).
[25] C. Helstrom, *Quantum Detection and Estimation Theory*, Mathematics in Science and Engineering (Academic Press, 1976).
[26] Supplementary Information.
[27] R. Demkowicz-Dobrzanski, U. Dorner, B. J. Smith, J. S. Lundeen, W. Wasilewski, K. Banaszek, and I. A. Walmsley, Phys. Rev. A, **80**, 013825 (2009).
[28] S. Knysh, V. N. Smelyanskiy, and G. A. Durkin, Phys. Rev. A, **83**, 021804 (2011).
[29] Z. Ji, G. Wang, R. Duan, Y. Feng, and M. Ying, Information Theory, IEEE Transactions on, **54**, 5172 (2008).
[30] G. Adesso, F. Dell'Anno, S. De Siena, F. Illuminati, and L. A. M. Souza, Phys. Rev. A, **79**, 040305 (2009).
[31] R. D. Gill and M. Guta, arxiv:1112.2078 (2011).
[32] S. Popoff, G. Lerosey, M. Fink, A. C. Boccara, and S. Gigan, Nature Comm., **1**, 81 (2010).
[33] A. Fedrizzi, R. Ursin, T. Herbst, M. Nespoli, R. Prevedel, T. Scheidl, F. Tiefenbacher, T. Jennewein, and A. Zeilinger, Nature Physics, **5**, 389 (2009).
[34] J. Kołodyński and R. Demkowicz-Dobrzański, Phys. Rev. A, **82**, 053804 (2010).

SUPPLEMENTARY INFORMATION

This supplement discusses in greater detail the technical aspects of the derivation of the results in the main text.

Quantum Cramér-Rao bound

The limit to the ultimate attainable precision of a set of parameters $\boldsymbol{\theta}$, their covariance matrix $\mathrm{Cov}(\boldsymbol{\theta})$, is given by the quantum version of the information inequality [25]

$$\mathrm{Cov}(\boldsymbol{\theta}) \geq (\mathcal{I}_{\boldsymbol{\theta}})^{-1}, \tag{8}$$

where $\mathcal{I}_{\boldsymbol{\theta}}$ is the quantum Fisher information matrix associated to the quantum state after evolution. This is a matrix inequality, and provides as a special case a lower bound on the achievable error for estimating any single parameter, which given by the Cramér-Rao inequality $(\Delta\theta_{\nu\nu})^2 \geq \mathcal{I}_{\nu\nu}^{-1}$ in terms of the quantum Fisher information $\mathcal{I}_{\nu\nu}$ [13]. For a single parameter θ_ν, the quantum Cramèr-Rao bound is always attainable, with the optimal measurement being given by the eigenvector of the symmetric logarithmic derivative (SLD) defined as

$$L_\nu \rho(\boldsymbol{\theta}) + \rho(\boldsymbol{\theta}) L_\nu = 2\frac{\partial \rho(\boldsymbol{\theta})}{\partial \theta_\nu}, \tag{9}$$

which also defines the quantum Fisher information matrix as $\mathcal{I}_{\mu\nu} = \Re\mathrm{Tr}\left[\rho(\boldsymbol{\theta}) L_\mu L_\nu\right]$. The precision in the estimate of the parameters is given by the saturation of the inequality in $\sum_\nu (\Delta\theta_{\nu\nu})^2 = \mathrm{Tr}\left[\mathrm{Cov}(\boldsymbol{\theta})\right] \geq \mathrm{Tr}\left[(\mathcal{I}_{\boldsymbol{\theta}})^{-1}\right]$. The classical multiparameter information inequality can always be achieved asymptotically using unbiased estimators, but in general, the quantum matrix equality in Eq. (8) cannot be achieved. This is due to the fact that the different SLDs L_ν, are not generally compatible, i.e. they do not satisfy the condition for weak commutativity [31]

$$\mathrm{Tr}\left[\rho(\boldsymbol{\theta})[L_\nu, L_\mu]\right] = 0. \tag{10}$$

Quantum Fisher information matrix

The orthogonal subspaces which the block diagonal submatrices of

$$\rho(\boldsymbol{\theta}) = \bigoplus_{l=0}^{n} p_l |\psi_l\rangle\langle\psi_l|.$$

occupy remain orthogonal under infinitesimal translations. Therefore, the SLD is similarly block diagonal with (see Supplementary Information)

$$L_\nu = \bigoplus_{l=0}^{N} L_\nu^l, \quad \text{with} \tag{11}$$

$$L_\nu^l = \Big(\partial_\nu \log p_l |\psi_l\rangle\langle\psi_l| + 2|\partial_\nu\psi_l\rangle\langle\psi_l| + 2|\psi_l\rangle\langle\partial_\nu\psi_l|\Big).$$

Given this block diagonal structure, the elements $\mathcal{I}_{\mu\nu}$ of the quantum Fisher information matrix are given by

$$\mathcal{I}_{\mu\nu}[\rho] = I_{\mu\nu}\left[\boldsymbol{p}\right] + \sum_{l=0}^{n} p_l \mathcal{I}_{\mu\nu}\left[|\psi_l\rangle\langle\psi_l|\right]. \tag{12}$$

The first term $I_{\mu\nu}[\boldsymbol{p}] = \sum_{l=0}^{n} p_l\, \partial_\mu \log p_l \partial_\nu \log p_l$ is the classical Fisher information matrix of the probability distribution $\boldsymbol{p}$. The second term, in some sense the 'purely quantum' contribution is the weighed quantum Fisher information of the constituent states $\mathcal{I}_{\mu\nu}[|\psi_l\rangle\langle\psi_l|] = 4\sum_{l=0}^{n} p_l(\Re P_{\mu\nu,l})$, where we use the shorthand

$$P_{\mu\nu,k} = \langle\partial_\mu\psi_k|\Pi_k|\partial_\nu\psi_k\rangle, \tag{13}$$

and the operator $\Pi_k = \mathbb{I} - |\psi_k\rangle\langle\psi_k|$ projects onto the subspace orthogonal to $|\psi_k\rangle$. For loss and phase estimation using states of the form Eq. (1), the quantum Fisher information matrix

$$\mathcal{I}[\rho] = \begin{pmatrix} \mathcal{I}_{\phi\phi} & \mathcal{I}_{\phi\eta} \\ \mathcal{I}_{\eta\phi} & \mathcal{I}_{\eta\eta} \end{pmatrix}, \tag{14}$$

is such that $\mathcal{I}_{\eta\phi} = \mathcal{I}_{\phi\eta} = 0$. The diagonals given by Eq. (3). Finally, the saturation of the multiparameter quantum Cramèr-Rao bound, governed by Eq. (10), reduces to

$$\mathrm{Tr}\left[\rho[L_\eta, L_\phi]\right] = i\sum_{l=0}^{n} p_l \left(\Im\langle\partial_\mu\psi_l|\partial_\nu\psi_l\rangle\right), \tag{15}$$

which in our case is, in general, nonzero as shown in Eq. (4). When estimating both the parameters using as measurement the eigenvectors of the SLD for phase L_ϕ, the precision for phase estimation scales at the quantum limit given by $\mathcal{I}_{\phi\phi}$. That of estimating the loss parameter is governed by the classical Fisher information [26] $I_{\eta\eta} = \sum_{l=0}^{n} p_l \left(\partial_\eta p_l\right)^2$.

Fixed-photon-number states

Consider pure quantum probe states with fixed resources, which in our case is the photon number, to estimate simultaneously the loss and phase in the interferometer in Fig. (1). We model the loss as a beam splitter of transmissivity η, resulting in a loss mode $|l\rangle_L$. The loss transforms the basis vectors as $|k, n-k\rangle \mapsto \sum_{l=0}^{k} \sqrt{b_l^k}|k-l, n-k\rangle \otimes |l\rangle_L$, where the coefficients b_l^k are given by $b_l^k = \begin{pmatrix} k \\ l \end{pmatrix} \eta^{k-l}(1-\eta)^l$. Including the phase accumulation, the final state is given by

$$|\psi\rangle = \sum_{k=0}^{n} \alpha_k e^{ik\phi} \sum_{l=0}^{k} \sqrt{b_l^k}|k-l, n-k\rangle \otimes |l\rangle_L, \tag{16}$$

with $\sqrt{x_k} = \alpha_k$. As the information of the photons lost cannot be recovered, tracing over the mode L leads to $\rho = \sum_{l=0}^{n} p_l |\psi_l\rangle\langle\psi_l|$, where the normalised states $|\psi_l\rangle$ are given by

$$|\psi_l\rangle = \frac{1}{\sqrt{p_l}} \sum_{k=l}^{n-l} \alpha_k \sqrt{b_l^k} e^{ik\phi}|k-l, n-k\rangle. \tag{17}$$

Owing to the orthogonality of the states $\langle\psi_l|\psi_{l'}\rangle = \delta_{ll'}$, the density matrix can be represented as a direct sum as [27]

$$\rho = \bigoplus_{l=0}^{n} p_l |\psi_l\rangle\langle\psi_l|. \tag{18}$$

Furthermore if the state vectors $|\psi_i\rangle$ remain orthogonal under infinitesimal translations $\theta_\kappa \mapsto \theta_\kappa + \mathrm{d}\theta_\kappa$, that is $(i \neq j)\langle\partial_\kappa\psi_i|\psi_j\rangle = 0$, and the derivative $\partial_\kappa\rho_{\boldsymbol{\theta}}$ and L_κ decompose into diagonal blocks $\partial_\kappa\rho_{i,\boldsymbol{\theta}}$ and $L_{i,\kappa}$ supported on the same orthogonal subspaces as the $\rho_{i,\boldsymbol{\theta}}$. This decomposition entails that eigenvalues of L_κ are those of the blocks L^i_κ. Each block has two non-zero eigenvalues

$$\lambda_{i,\kappa} = \frac{1}{2}\left(\partial_\kappa \log p_i \pm \sqrt{(\partial_\kappa \log p_i)^2 + 16P_{i,\kappa\kappa}}\right) \tag{19}$$

with corresponding eigenvectors

$$|\lambda_{i,\kappa}\rangle = \frac{\lambda_{i,\kappa}\sqrt{P_{i,\kappa\kappa}}|\psi_i\rangle + 2\mathbb{P}_i|\partial_\kappa\psi_i\rangle}{\sqrt{P_{i,\kappa\kappa}(\lambda^2_{i,\kappa} + 4P_{i,\kappa\kappa})}} \tag{20}$$

where $P_{i,\mu\nu} = \langle\partial_\mu\psi_i|\mathbb{P}_i|\partial_\nu\psi_i\rangle$, and the operator $\mathbb{P}_i = \mathbb{I} - |\psi_i\rangle\langle\psi_i|$ projects into the space perpendicular to $|\psi_i\rangle$.

Now consider the strategy in which measurements are made by projecting $\rho_{\boldsymbol{\theta}}$ onto the eigenvectors of L_κ, thus saturating the quantum Cramér-Rao bound for estimation of θ_κ. Generally, however, the elements of the Fisher information matrix for estimation in this basis $I_{\mu\nu}(\theta_\kappa)$ deviate from the quantum bound $\mathcal{I}_{\mu\nu}$,

$$I_{\mu\nu}(\theta_\kappa) = \sum_i p_i\left(\partial_\mu \log p_i \partial_\nu \log p_i + \frac{4\Re P_{i,\kappa\mu}\Re P_{i,\kappa\nu}}{P_{i,\kappa\kappa}}\right), \tag{21}$$

where the first term represents 'classical' information, and the second term makes the 'truly quantum' contribution. For comparison the corresponding quantum Fisher information matrix is given by

$$\mathcal{I}_{\mu\nu} = \sum_i p_i\left(\partial_\mu \log p_i \partial_\nu \log p_i + 4\Re P_{i,\mu\nu}\right). \tag{22}$$

Derivation of Fisher information matrices

The state is given by Eqns.(17) and (18). The Fisher information matrices for states of this form are given by (21) and (22). In what follows,

$$\xi_{r,s} = \sum_{t=s}^{n} x_t b^t_s t^r, \quad \Xi_r = \sum_{s=0}^{n}\xi_{r,s} = \sum_{t=0}^{n} x_t t^r, \tag{23}$$

are the moments of the coefficients of $x_t = |\alpha_t|^2$, with the constraint $\sum_{t=0}^{n} x_t = 1$, and b^t_s is the binomial factor defined in the last section. We begin by reexpressing the probabilities as

$$p_l = p_l\langle\psi_l|\psi_l\rangle = \sum_{k=l}^{n}|\alpha_k|^2 b^k_l = \sum_{k=l}^{n} x_k b^k_l = \xi_{0,l}. \tag{24}$$

Evaluating the relevant inner products gives

$$\langle\psi_l|\partial_\phi\psi_l\rangle = i\sum_{k=l}^{n}\frac{k|\alpha_k|^2 b^k_l}{p_l} = i\frac{\xi_{1,l}}{\xi_{0,l}}, \tag{25a}$$

$$\langle\partial_\phi\psi_l|\partial_\phi\psi_l\rangle = \sum_{k=l}^{n}\frac{k^2|\alpha_k|^2 b^k_l}{p_{l0}} = \frac{\xi_{2,l}}{\xi_{0,l}}, \tag{25b}$$

$$\langle\psi_l|\partial_\eta\psi_l\rangle = \sum_{k=l}^{n}\alpha^*_k e^{-ik\phi}\sqrt{\frac{b^k_l}{p_l}}\partial_\eta\left(\alpha_k e^{ik\phi}\sqrt{\frac{b^k_l}{p_l}}\right) = $$
$$= \frac{1}{2}\partial_\eta\left(\frac{1}{\xi_{0,l}}\sum_{k=l}^{n} x_k b^k_l\right) = 0. \tag{25c}$$

This reflects the geometry of the estimation problem, wherein the η derivative is orthogonal to the initial state,

$$\langle\partial_\eta\psi_l|\partial_\eta\psi_l\rangle = \sum_{k=l}^{n}\partial_\eta\left(\frac{\alpha^*_k e^{-ik\phi}\sqrt{b^k_l}}{\sqrt{p_l}}\right)\partial_\eta\left(\frac{\alpha_k e^{ik\phi}\sqrt{b^k_l}}{\sqrt{p_l}}\right)$$
$$= \sum_{k=l}^{n}|\alpha_k|^2\left(\partial_\eta\sqrt{\frac{b^k_l}{p_l}}\right)^2 = \frac{\xi_{2,l}\xi_{0,l} - \xi^2_{1,l}}{4\eta^2\xi^2_{0,l}}, \tag{25d}$$

$$\langle\partial_\phi\psi_l|\partial_\eta\psi_l\rangle = -i\sum_{k=l}^{N} k\alpha^*_k e^{-ik\phi}\sqrt{\frac{b^k_l}{p_l}}\partial_\eta\left(\alpha_k e^{ik\phi}\sqrt{\frac{b^k_l}{p_l}}\right)$$
$$= -i\frac{\xi_{2,l}\xi_{0,l} - \xi^2_{1,l}}{2\eta\xi^2_{0,l}}. \tag{25e}$$

Writing these in the shorthand $P_{k,\mu\nu} = \langle\partial_\mu\psi_k|\partial_\nu\psi_k\rangle - \langle\partial_\mu\psi_k|\psi_k\rangle\langle\psi_k|\partial_\nu\psi_k\rangle$ introduced in the last section, we find

$$P_{l,\phi\phi} = \frac{\xi_{2,l}\xi_{0,l} - \xi^2_{1,l}}{\xi^2_{0,l}}, \; P_{l,\eta\eta} = \frac{\xi_{2,l}\xi_{0,l} - \xi^2_{1,l}}{4\eta^2\xi^2_{0,l}} \tag{26a}$$

$$P_{l,\phi\eta} = \frac{\xi_{2,l}\xi_{0,l} - \xi^2_{1,l}}{2i\eta\xi^2_{0,l}}. \tag{26b}$$

Also required is the Fisher information of the distribution $\{p_l\}$, given by the terms $\langle\partial_\mu \log p_l \partial_\nu \log p_l\rangle$. In order to evaluate these one needs to use some properties of $\xi_{n,l}$, including

$$\partial_\eta b^k_l = b^k_l\left(\frac{k}{\eta} - \frac{l}{\eta(1-\eta)}\right) \tag{27a}$$

$$\partial_\eta\xi_{i,l} = \left(\frac{\xi_{i+1,l}}{\eta} - \frac{l\xi_{i,l}}{\eta(1-\eta)}\right) \tag{27b}$$

$$\sum_{l=0}^{n}\xi_{i,l} = \Xi_i, \quad \sum_{l=0}^{n}\frac{l\xi_{i,l}}{1-\eta} = \Xi_{i+1} \tag{27c}$$

$$\sum_{l=0}^{n}\frac{l^2\xi_{i,l}}{(1-\eta)^2} = \Xi_{i+2} + \frac{\eta}{1-\eta}\Xi_{i+1} \tag{27d}$$

These relations can be used to evaluate

$$\langle\partial_\eta \log p_l\, \partial_\eta \log p_l\rangle = \sum_{l=0}^{n}\frac{1}{p_l}(\partial_\eta p_l)^2 = \sum_{l=0}^{n}\frac{1}{\xi_{0,l}}(\partial_\eta\xi_{0,l})^2$$
$$= \frac{1}{\eta(1-\eta)}\Xi_1 - \frac{1}{\eta^2}\left(\Xi_2 - \sum_{l=0}^{n}\frac{\xi^2_{1,l}}{\xi_{0,l}}\right).$$

The other products are much simpler and follow trivially from $\partial_\phi p_l = 0$. That is, $\langle \partial_\phi \log p_l \, \partial_\phi \log p_l \rangle = 0, \langle \partial_\phi \log p_l \, \partial_\eta \log p_l \rangle = 0$. Although derived for the loss and the phase parameters here, this general feature for any pair of parameters corresponding to hamiltonian and dissipative dynamics.

Combining these results, the quantum Fisher information matrix elements from Eq. (22) are thus given by

$$\begin{aligned}\mathcal{I}_{\phi\phi} &= \sum_{l=0}^{n} p_l \left((\partial_\phi \log p_l)^2 + 4\Re P_{l,\phi\phi} \right) \\ &= 4\sum_{l=0}^{n} \frac{1}{\xi_{0,l}} \left(\xi_{2,l}\xi_{0,l} - \xi_{1,l}^2 \right) = 4\left(\Xi_2 - \sum_{l=0}^{n} \frac{\xi_{1,l}^2}{\xi_{0,l}} \right) \end{aligned} \tag{29a}$$

$$\begin{aligned}\mathcal{I}_{\eta\eta} &= \sum_{l=0}^{n} p_l \left((\partial_\eta \log p_l)^2 + 4\Re P_{l,\eta\eta} \right) \\ &= \frac{\Xi_1}{\eta(1-\eta)} - \frac{1}{\eta^2}\left(\Xi_2 - \sum_{l=0}^{n} \frac{\xi_{1,l}^2}{\xi_{0,l}} \right) + \sum_{l=0}^{n} \frac{\left(\xi_{2,l}\xi_{0,l} - \xi_{1,l}^2 \right)}{\eta^2 \xi_{0,l}} \end{aligned} \tag{29b}$$

$$= \frac{1}{\eta(1-\eta)}\Xi_1$$

$$\mathcal{I}_{\eta\phi} = \mathcal{I}_{\phi\eta} = 0 \tag{29c}$$

When evaluating the Fisher information matrix elements given by Eq. (21) for the estimation using the optimal measurements for ϕ, we obtain the same forms for $\mathcal{I}$ except $\mathcal{I}_{\eta\eta}$ where the useful cancelation which occurs in Eq. (29a) no longer occurs.

$$I_{\phi\phi}^{L_\phi} = 4\sum_{l=0}^{n} \frac{1}{\xi_{0,l}} \left(\xi_{2,l}\xi_{0,l} - \xi_{1,l}^2 \right) = 4\left(\Xi_2 - \sum_{l=0}^{n} \frac{\xi_{1,l}^2}{\xi_{0,l}} \right)$$

$$I_{\eta\eta}^{L_\phi}(\phi) = \frac{1}{\eta(1-\eta)}\Xi_1 - \frac{1}{\eta^2}\left(\Xi_2 - \sum_{l=0}^{n} \frac{\xi_{1,l}^2}{\xi_{0,l}} \right) \tag{30a}$$

$$I_{\eta\phi}^{L_\phi}(\phi) = I_{\phi\eta}^{L_\phi}(\phi) = 0 \tag{30b}$$

Also of interest is estimation using the optimal measurements for η. One finds that since $P_{l,\eta\phi}$ purely imaginary, and p_l carries no ϕ dependence, so $I_{\phi\phi}^{L_\eta} = I_{\eta\phi}^{L_\eta} = I_{\phi\eta}^{L_\eta} = 0$, and

$$I_{\eta\eta}^{L_\eta} = \frac{\Xi_1}{\eta(1-\eta)}. \tag{31}$$

A final result that is of some significance is the condition for commutativity of SLDs [31]. In terms of the shorthand introduced in the last section, it is

$$\mathrm{Tr}\left[\rho \left(L_\mu L_\nu - L_\nu L_\mu \right)\right] = 4i\sum_{l=0}^{n} p_l \Im P_{l,\mu\nu}, \tag{32}$$

which for the case of simultaneous estimation of η and ϕ, using the results of (24), (25) and (26), is

$$\begin{aligned}\mathrm{Tr}\left[\rho \left(L_\eta L_\phi - L_\phi L_\eta \right)\right] &= 4\sum_{l=0}^{n} \frac{1}{2\eta\xi_{0,l}} \left(\xi_{2,l}\xi_{0,l} - \xi_{1,l}^2 \right) \\ &= -i\frac{2}{\eta}\left(\Xi_2 - \sum_{l=0}^{n} \frac{\xi_{1,l}^2}{\xi_{0,l}} \right). \end{aligned} \tag{33}$$

Asymptotic profile

This section provides a step by step derivation of the asymptotic results in the high loss, high flux regime. We begin with the expressions for the quantum Fisher information for phase and loss estimation given by Eqns. (29a) and (29b). We first separate $\mathcal{I}_{\phi\phi}$ into its constituent terms after having shifted the mean by a constant

$$\begin{aligned}\mathcal{I}_{\phi\phi} = 4\Bigg[&\sum_{l=0}^{n}\sum_{k=l}^{N} b_l^k \left(k - \frac{l}{1-\eta} \right)^2 |\alpha_k|^2 \\ &- \sum_{l=0}^{n} \frac{1}{p_{l0}} \left[\sum_{k=l}^{n} b_l^k \left(k - \frac{l}{1-\eta} \right) |\alpha_k|^2 \right]^2 \Bigg] \end{aligned} \tag{34}$$

By considering only the first term, and noting that the second term is a positive quantity, one obtains an upper bound for $\mathcal{I}_{\phi\phi}$

$$\sum_{l=0}^{n}\sum_{k=l}^{n} b_l^k \left(k - \frac{l}{1-\eta} \right)^2 |\alpha_k|^2 = \frac{\eta}{1-\eta}\sum_{k=0}^{n} k\,|\alpha_k|^2 \tag{35}$$

In the limit of large n, it is reasonable to approximate the sums by integrals with $k = nz = n(1-y)$ and $|\alpha_k|^2 = \alpha^2(z)\mathrm{d}z = -f^2(1-z)\mathrm{d}z = f^2(y)\mathrm{d}y$. This implies $x_k = |\alpha_k|^2 \mapsto \frac{1}{n}\alpha^2(k/n) \mapsto \frac{1}{n}f^2(1-k/n)$

$$\sum_{k=0}^{N} k\,|\alpha_k|^2 \approx \int_0^N k\,|\alpha_k|^2\,\mathrm{d}k = n\int_0^1 (1-y)f^2(y)\mathrm{d}y. \tag{36}$$

Under this transformation the normalisation condition transforms as follows

$$1 = \langle\psi|\psi\rangle = \sum_{k=0}^{n} |\alpha_k|^2 \approx \int_0^n |\alpha_k|^2\,\mathrm{d}k = \int_0^1 f^2(y)\mathrm{d}y. \tag{37}$$

Hence by Eqns. (35) and (36), the first term of Eq. (34) is

$$\begin{aligned}\frac{\eta}{1-\eta}\sum_{k=0}^{n} k\,|\alpha_k|^2 &\approx \frac{n\eta}{1-\eta}\int_0^1 (1-y)f^2(y)\mathrm{d}y \\ &= \frac{n\eta}{1-\eta}\left(1 - \int_0^1 y f^2(y)\mathrm{d}y \right). \end{aligned} \tag{38}$$

Now consider the normalisation constants $p_l = \sum_{n=l}^{N} b_l^k |\alpha_k|^2$. The continuous limit is taken using the de Moivre-Laplace theorem. Under the added condition that $l \approx k(1-\eta)$ as $k \to \infty$

$$b_l^k \approx \frac{1}{\sqrt{2\pi k\eta(1-\eta)}} \exp\left(-\frac{(l-k(1-\eta))^2}{2k\eta(1-\eta)} \right). \tag{39}$$

This leads to

$$\begin{aligned} p_l &\approx \int_l^n \frac{1}{\sqrt{2\pi k\eta(1-\eta)}} \exp\left(-\frac{(l-k(1-\eta))^2}{2k\eta(1-\eta)} \right) |\alpha_k|^2\,\mathrm{d}k \\ &= \int_{\frac{l}{n}}^1 \frac{1}{n(1-\eta)\sqrt{2\pi\sigma^2}} \sqrt{\frac{\mu}{z}} \exp\left(-\frac{\mu}{z}\frac{(z-\mu)^2}{2\sigma^2} \right) \alpha^2(z)\,\mathrm{d}z \\ &\approx \int_{\frac{l}{n}}^1 \frac{1}{n(1-\eta)\sqrt{2\pi\sigma^2}} \exp\left(-\frac{(z-\mu)^2}{2\sigma^2} \right) \alpha^2(z)\,\mathrm{d}z \end{aligned} \tag{40}$$

where $\mu = \frac{l}{n(1-\eta)}$, $\sigma^2 = \frac{l\eta}{n^2(1-\eta)^2}$ and the last approximation is near equality for $\mu \gg \sigma$. A Taylor expansion to the first order $\alpha^2(z) = \left(\alpha(\mu) + \alpha'(\mu)(z-\mu) + \mathcal{O}(z-\mu)^2\right)^2 = \alpha^2(\mu) + 2\alpha(\mu)\alpha'(\mu)(z-\mu) + \mathcal{O}(z-\mu)^2$ substitution into the integral, and taking the limit to infinity leads to the first order term being zero by parity. Due to the sharpness of the distribution, the limits can be taken to infinity.

$$p_l \approx \frac{\alpha^2(\mu)}{n(1-\eta)} \int_{-\infty}^{\infty} \frac{1}{\sqrt{2\pi\sigma^2}} \exp\left(-\frac{(z-\mu)^2}{2\sigma^2}\right) \mathrm{d}z = \frac{\alpha^2(\mu)}{n(1-\eta)}.$$

Using the approximation given in Eq. (39) to obtain a continuous limit form for the second term in Eq. (34) leads to

$$\begin{aligned}
\sum_{k=l}^{n} b_l^k \left(k - \frac{l}{1-\eta}\right) |\alpha_k|^2 &\approx \int_l^n \left(\frac{1}{\sqrt{2\pi k\eta(1-\eta)}} \exp\left[-\frac{(l-k(1-\eta))^2}{2k\eta(1-\eta)}\right] \left(k - \frac{l}{(1-\eta)}\right) |\alpha_k|^2\right) \mathrm{d}k \\
&= \int_{\frac{l}{n}}^1 \left(\frac{1}{(1-\eta)\sqrt{2\pi\sigma^2}} \sqrt{\frac{\mu}{z}} \exp\left[-\frac{\mu}{z}\frac{(z-\mu)^2}{2\sigma^2}\right] (z-\mu)\alpha^2(z)\right) \mathrm{d}z \\
&\approx \int_{\frac{l}{n}}^1 \frac{1}{(1-\eta)\sqrt{2\pi\sigma^2}} \exp\left[-\frac{(z-\mu)^2}{2\sigma^2}\right] (z-\mu)\alpha^2(z)\,\mathrm{d}z,
\end{aligned} \tag{41}$$

where the same values of $\mu = \frac{l}{n(1-\eta)}$ and $\sigma^2 = \frac{l\eta}{n^2(1-\eta)^2}$ are used. When the limit is taken to infinity in this integral one loses the zeroth order term of the Taylor expansion by parity and retaining the first order term

$$\begin{aligned}
&\sum_{k=l}^{n} b_l^k \left(k - \frac{l}{1-\eta}\right) |\alpha_k|^2 \\
&\approx \frac{1}{1-\eta} \int_{-\infty}^{\infty} \frac{1}{\sqrt{2\pi\sigma^2}} \exp\left(-\frac{(z-\mu)^2}{2\sigma^2}\right) (z-\mu)\alpha^2(z)\,\mathrm{d}z \\
&\approx \frac{2\alpha(\mu)\alpha'(\mu)}{1-\eta} \int_{-\infty}^{\infty} \frac{1}{\sqrt{2\pi\sigma^2}} \exp\left(-\frac{(z-\mu)^2}{2\sigma^2}\right) (z-\mu)^2 \mathrm{d}z \\
&= \frac{2\alpha(\mu)\alpha'(\mu)\sigma^2}{1-\eta}.
\end{aligned} \tag{42}$$

The second term in Eq. (34) is then

$$\begin{aligned}
&\frac{1}{p_l} \left[\sum_{k=l}^{n} b_l^k \left(k - \frac{l}{1-\eta}\right) |\alpha_k|^2\right]^2 \\
&= \frac{n(1-\eta)}{\alpha^2(\mu)} \left[\frac{2\alpha(\mu)\alpha'(\mu)\sigma^2}{1-\eta}\right]^2 \\
&= \alpha'^2\left(\frac{l}{n(1-\eta)}\right) \frac{4n}{1-\eta} \left(\frac{l\eta}{n^2(1-\eta)^2}\right)^2.
\end{aligned} \tag{43}$$

Taking the sum over l to the continuous limit, one obtains

$$\begin{aligned}
&\sum_{l=0}^{n} \frac{1}{p_l} \left[\sum_{k=l}^{n} b_l^k \left(k - \frac{l}{1-\eta}\right) |\alpha_k|^2\right]^2 \\
&= \int_0^N \alpha'^2\left(\frac{l}{n(1-\eta)}\right) \frac{4n}{1-\eta} \left(\frac{l\eta}{n^2(1-\eta)^2}\right)^2 \mathrm{d}l \\
&= 4n^2 \left(\frac{\eta}{n(1-\eta)}\right)^2 \int_0^{\frac{1}{1-\eta}} z^2 \alpha'^2(z)\mathrm{d}z \\
&= 4\left(\frac{\eta}{1-\eta}\right)^2 \int_{\frac{-\eta}{1-\eta}}^1 (1-y)^2 f'^2(y)\mathrm{d}y,
\end{aligned} \tag{44}$$

Putting together Eqns. (38) and (44), one obtains an asymptotic form for Eq. (34)

$$\begin{aligned}
\mathcal{I}_{\phi\phi} = 4\Big[&\frac{n\eta}{1-\eta}\left(1 - \int_0^1 y f^2(y)\mathrm{d}y\right) \\
&- 4\left(\frac{\eta}{1-\eta}\right)^2 \int_{\frac{-\eta}{1-\eta}}^1 (1-y)^2 f'^2(y)\mathrm{d}y\Big].
\end{aligned} \tag{45}$$

Taking the upper bound of both integrals to infinity, the lower bound of the second integral go to zero, and using that the distribution is sharply peaked around $y \approx 0$ in the second integrand one obtains the final form

$$\mathcal{I}_{\phi\phi} \approx \frac{4n\eta}{1-\eta}\left[1 - \int_0^\infty \left(yf^2(y) + \frac{4\eta}{n(1-\eta)}f'^2(y)\right)\mathrm{d}y\right]. \tag{46}$$

Using similar techniques

$$\begin{aligned}\mathcal{I}_{\eta\eta} &= \frac{1}{\eta(1-\eta)}\sum_{n=0}^{n} k\,|\alpha_k|^2 \\ &\approx \frac{n}{\eta(1-\eta)}\left[1 - \int_0^\infty yf^2(y)\mathrm{d}y\right].\end{aligned} \tag{47}$$

Therefore,

$$I_{\eta\eta} = \mathcal{I}_{\eta\eta} - \frac{1}{4\eta^2}\mathcal{I}_{\phi\phi} = \frac{4}{(1-\eta)^2}\left[\int_0^\infty f'^2(y)\mathrm{d}y\right]. \tag{48}$$

The final task is to maximize a convex combinations of the Fisher informations for phase and in Eqns. (46) and (48) with a weight $0 \leq w \leq 1$ assigned to $\mathcal{I}_{\phi\phi}$. The two quantities however scale differently with n and η. Consequently, a maximisation of their combination is unduly weighed by one of the quantities. To circumvent this, the Fisher information for the two parameters should be rescaled by their respective maxima, given by $\mathcal{I}_{\phi\phi}^{\max} = 4n\eta/(1-\eta)$, and $I_{\eta\eta}^{\max} = n/\eta(1-\eta)$. The final quantity to be maximized is given by

$$\begin{aligned}&w\frac{\mathcal{I}_{\phi\phi}}{\mathcal{I}_{\phi\phi}^{\max}} + (1-w)\frac{I_{\eta\eta}}{I_{\eta\eta}^{\max}} \\ &= w\left[1 - \int_0^\infty \left(yf^2(y) + \gamma^3 f'^2(y)\right)\mathrm{d}y\right]\end{aligned} \tag{49}$$

with $\gamma^3 = \left(2 - \frac{1}{w}\right)\frac{4\eta}{n(1-\eta)^2}$, which is equivalent to minimizing the integrand when provided $w > 1/2$. In that case, the Euler-Lagrange method leads to the differential equation

$$yf(y) = \gamma^3 \frac{\mathrm{d}^2 f(y)}{\mathrm{d}y^2}, \tag{50}$$

subject to the normalisation condition and the initial condition $f'(0) = 0$. The solution is an Airy function, in particular

$$f(y) = \sqrt{\frac{1}{\gamma|\zeta_0|\mathrm{Ai}^2(\zeta_0)}}\mathrm{Ai}\left(\frac{y}{\gamma} + \zeta_0\right), \tag{51}$$

where $\zeta_0 = -1.01879$ is the first zero of the first derivative if the Airy function, i.e., $\mathrm{Ai}'(\zeta_0) = 0$. Reverting to the quantities of original interest,

$$x_k \approx \frac{1}{n\gamma|\zeta_0|\mathrm{Ai}^2(\zeta_0)}\mathrm{Ai}^2\left(\frac{1}{\gamma} - \frac{k}{\gamma n} + \zeta_0\right), \tag{52}$$

and

$$\mathcal{I}_{\phi\phi} = (1 - \gamma|\zeta_0|)\mathcal{I}_{\phi\phi}^{\max}, \quad I_{\eta\eta} = \left(\frac{4|\zeta_0|}{3\gamma^2}\right)I_{\eta\eta}^{\max}. \tag{53}$$